

Semi-classical equation of state and specific heats for neutron-star inner crust with proton shell corrections.

M. Onsi,¹ A. K. Dutta,^{1,2} H. Chatri,¹ S. Goriely,³ N. Chamel,³ and J. M. Pearson¹

¹*Dépt. de Physique, Université de Montréal,
Montréal (Québec), H3C 3J7 Canada*

²*School of Physics, Devi Ahilya University, Indore 452001, India*

³*Institut d'Astronomie et d'Astrophysique,
Université Libre de Bruxelles - CP226, 1050 Brussels, Belgium*

Abstract

An approach to the equation of state for the inner crust of neutron stars based on Skyrme-type forces is presented. Working within the Wigner-Seitz picture, the energy is calculated by the TETF (temperature-dependent extended Thomas-Fermi) method, with proton shell corrections added self-consistently by the Strutinsky-integral method. Using a Skyrme force that has been fitted to both neutron matter and to essentially all the nuclear mass data, we find strong proton shell effects: proton numbers $Z = 50, 40$ and 20 are the only values possible in the inner crust, assuming that nuclear equilibrium is maintained in the cooling neutron star right down to the ambient temperature.

Convergence problems with the TETF expansion for the entropy, and our way of handling them, are discussed. Full TETF expressions for the specific heat of inhomogeneous nuclear matter are presented. Our treatment of the electron gas, including its specific heat, is essentially exact, and is described in detail.

PACS numbers: 21.10.Dr, 21.60.Jz, 21.65+f, 26.60.+c

I. INTRODUCTION

We are concerned with the application of Skyrme-type effective nuclear interactions to the determination of the equation of state (EOS) of the inhomogeneous nuclear matter encountered at nuclear and subnuclear densities in core-collapse supernovas and in the inner crust of neutron stars. In our first paper on this topic [1] we adopted a Wigner-Seitz (WS) model of the inhomogeneous nuclear medium, and used the fourth-order semi-classical temperature-dependent extended Thomas-Fermi (TETF) method to calculate the kinetic energy and entropy. That paper dealt primarily with the conditions prevailing in core-collapse supernovas. The present paper relates rather to the inner crust of neutron stars, describing in particular some modifications to the earlier model, made necessary by two problems that emerge at the much lower temperatures T that are involved: i) the TETF expansion (in powers of \hbar^2) for the entropy converges badly at low T ; ii) proton shell effects are not negligible at low T .

This last point is especially important if one is interested in the neutron-star crust as a possible alternative site for the synthesis of the so-called r-process elements [2, 3, 4, 5]. The usual model of the r-process of nucleosynthesis is associated with the *birth* of a neutron star in a core-collapse supernova, during which “seed” nuclei are exposed to an intense flux of neutrons. Rapid (“*r*”) capture of neutrons alternating with beta decay leads to the formation of a string of highly neutron-rich isotopes of a wide range of elements, which, once the source of neutrons is removed, will beta-decay back to the most neutron-rich stable isobar for the given mass number A (see Ref. [6] for a recent review). The alternative picture, of interest here, is associated rather with the *death* of a neutron star, or at least with its partial disruption. Because of the very large densities, the matter in a neutron star is highly neutron rich, and the closer to the center the more neutron-rich it will be. But if for one reason or another matter is ejected from the neutron star it will rapidly decompress, and so will be able to undergo a chain of beta decays, the end-product of which will again be r-process nuclei. Ejection of matter from a neutron star is usually supposed to result from the merger of one neutron star with another, or with a black hole [4, 7], but other scenarios have been envisaged, e.g., volcanoes [8], magnetars [9], quark stars [10] and explosions resulting from the mass of the neutron star falling below the minimal critical value [11]. However, the precise ejection mechanism is of no concern to us in this paper.

It is convenient at this point to recall that at least three distinct regions can be recognized in a neutron star: a central, locally homogeneous, core, and two concentric shells characterized by different inhomogeneous phases [12]. The outermost of these shells, the “outer crust”, consists of an electrically neutral lattice of nuclei and electrons. At the surface of the star only nuclei that are stable under natural terrestrial conditions are found (in fact, nuclear equilibrium, discussed below, implies that only ^{56}Fe will be found), but on moving towards the interior the increasing density leads to the appearance of nuclei that are more and more neutron rich, until at a mean local density $\bar{\rho}$ of around 2.4×10^{-4} nucleons.fm $^{-3}$ (4.0×10^{11} g.cm $^{-3}$) neutron drip sets in. This marks the transition to the “inner crust”, which at least up to a mean density of $\bar{\rho} = 0.06$ nucleons.fm $^{-3}$ consists of neutron-proton clusters, or droplets, immersed in a neutron gas, with the neutralizing electron gas being essentially uniform (we neglect screening effects in this paper). It is equally well established that by the point where the mean density has risen to around $\bar{\rho} = 0.10$ nucleons.fm $^{-3}$, i.e., about 2/3 of the density ρ_0 of symmetric infinite nuclear matter (INM) at equilibrium, the droplet phase no longer exists and has been replaced by the homogeneous phase of the core, which consists primarily of neutrons, with a small admixture of proton-electron pairs, and possibly other particles, including free quarks, closer to the center.

What happens in the transition region over the range $0.06 \leq \bar{\rho} \leq 0.10$ nucleons.fm $^{-3}$, close to the inside edge of the inner crust, is far less clear. The question cannot be settled by observation at the present time, and theoretical predictions are sensitive to the details of the calculations, in particular to the choice of the effective interaction. For some interactions the transition from the droplet phase to the homogeneous phase is indirect and complex, with a whole sequence of different inhomogeneous phases being formed. At the interface with the homogeneous core these calculations find a “bubble” phase, this taking the form of bubbles of neutron gas in a denser liquid of neutrons and protons, the droplet phase having effectively been turned inside out. Furthermore, at slightly lower densities, between the bubble and droplet phases, several so-called “pasta” phases are predicted to put in an appearance, these being characterized by exotic, non-spherical shapes [12]. On the other hand, it has been shown that for other effective interactions the situation is much simpler, with no bubble or pasta phases being formed (at least at the assumed zero temperature of a stable neutron star): at a mean density of around $\bar{\rho} = 0.075$ nucleons.fm $^{-3}$ the droplet phase undergoes a transition directly to the homogeneous phase (see Ref. [13], and references cited therein; also

Ref. [14]). In the present paper we will avoid these ambiguities by limiting ourselves to values of $\bar{\rho}$ less than $0.06 \text{ nucleons.fm}^{-3}$, which means that we would not be able to deal with ejection mechanisms that reached even deeper into the star.

Since neutron stars are formed at temperatures of the order of 10 MeV (10^{11} K) and rapidly cool to around 0.1 MeV [12], it is usually assumed that the final composition of the stable star corresponds to nuclear and beta equilibrium at a temperature of $T = 0$, the configuration of so-called “cold catalyzed matter”; we shall later examine the validity of this assumption. Determining the composition of the outer crust in this picture is straightforward (see, for example, Ref. [15]): the equilibrating nucleus at each given density (or pressure) is found from the known nuclear masses, as given by experiment or, where mass data are unavailable, a mass model such as the FRDM [16] or HFB-14 [17] (see also Refs. [18, 19] for reviews). We shall therefore not consider the outer crust any further here.

As for the composition of the inner crust of the stable neutron star, the relevant question at a given mean density $\bar{\rho}$ is to determine the total number of neutrons N , including those of the vapor, and protons Z per cluster. For this one needs the total Helmholtz free energy per nucleon f (including the electronic contribution) at the ambient temperature (usually taken to be zero), as a function of the density and the composition $X \equiv (Z, A = Z + N)$; one then minimizes f with respect to N and Z at constant $\bar{\rho}$. (Alternatively, to determine the composition at a given *pressure* P one minimizes the Gibbs free energy per nucleon g with respect to N and Z at constant P . It follows from the easily proven thermodynamical relation

$$\left(\frac{\partial g}{\partial X}\right)_{P,T} = \left(\frac{\partial f}{\partial X}\right)_{\bar{\rho},T} \quad (1.1)$$

that the two procedures are completely equivalent. We nevertheless find it more convenient to work with the Helmholtz free energy f at given values of $\bar{\rho}$: see, for example, Section II of Ref. [20].)

The pressure in a layer of the crust of density $\bar{\rho}$ can then be found by numerical differentiation from the identity

$$P = \bar{\rho}^2 \left(\frac{\partial f}{\partial \bar{\rho}}\right)_{T,X} \quad ; \quad (1.2)$$

note particularly that f is a mean quantity, averaged over inhomogeneities, and not a local quantity. With the pressure P determined as a function of the mean density $\bar{\rho}$, the values of

P and $\bar{\rho}$ in any layer of the neutron star, along with the local composition, can be determined through solution of the Tolman-Oppenheimer-Volkoff equation [21, 22].

When, for one reason or another, decompression of crustal material begins, the temperature may start to rise. To follow the evolution of this process we shall require the EOS for non-zero values of T , and also the specific heat per nucleon at constant volume, c_v , given in terms of the entropy per nucleon, s , by

$$c_v = T \left(\frac{\partial s}{\partial T} \right)_{\bar{\rho}, X} . \quad (1.3)$$

The entropy itself is given in terms of the Helmholtz free energy by

$$s = - \left(\frac{\partial f}{\partial T} \right)_{\bar{\rho}, X} . \quad (1.4)$$

Thus all quantities of interest here can be derived from a calculation of f as a function of $\bar{\rho}$ and T . Note that s and c_v , like f , are mean quantities.

A popular EOS that has been extensively applied to supernova explosions is that of Lattimer and Swesty [23]. However, the applicability of this EOS to neutron-star crusts is limited by the fact that it is based on the so-called compressible liquid-drop model without any shell corrections, which at the prevailing low temperatures can be expected to be significant. Actually, both Refs. [2] and [3] attempt to take account of shell effects, although in a rather rudimentary way, by making use of the algebraic bunching technique of Myers and Swiatecki [24].

In the present paper, as in Ref. [1], we model the inhomogeneous nuclear medium by a single spherical WS cell, and attempt to incorporate shell effects into this framework microscopically and self-consistently, thereby permitting some measure of continuity of treatment across the interface between the inner and outer crusts. The most obvious way to do this is through the Hartree-Fock (HF) method, as has already been done, for example, by Bonche and Vautherin [25] at finite temperature and by Negele and Vautherin [26] at zero temperature, using the WS approximation. However, we abandoned this approach for the following reason. While protons are strongly bound in the inner crust because of the large neutron excess, and thus show strong shell effects, for neutrons, by the very definition of the inner crust, there will be a continuous spectrum of unbound single-particle (s.p.) neutron states that are occupied. Thus any neutron added to the system must in reality go into this continuum, whence it follows that we should not expect any neutron shell effects. Actually,

this conclusion will hold only if the dripped neutrons form a uniform liquid, and in reality scattering of unbound neutrons on the inhomogeneities of the crust may give rise to so-called Casimir or band effects[27, 28, 29], whose exact evaluation requires the application of the band theory of solids (see Ref. [30] and references quoted therein). Nevertheless, these neutron shell effects are much smaller than the proton ones [31] and have therefore a negligible impact on the EOS and the equilibrium composition of the inner crust, although they are known to be significant for transport properties [32]. However, in practice any HF calculation in the WS approximation involves discretization, giving rise to shell effects for both protons and neutrons. But, as we have argued above, these neutron shell effects must be spurious, and in the HF calculation of Ref. [26] special steps had to be taken to smooth them (see also Refs. [30, 33]). We conclude that as far as neutrons are concerned the semiclassical extended Thomas-Fermi method is better adapted to a WS approach than is the HF method.

The solution we adopt here to the problem of including the appropriate proton shell corrections without introducing spurious neutron shell corrections is to use the ETFSI (extended Thomas-Fermi plus Strutinsky integral) high-speed approximation to the HF method [34, 35, 36, 37, 38]. We have already made an exploratory study of the applicability of this method to a WS picture of the EOS, and found that proton shell effects are indeed important [39], but here, in addition to making much more extensive calculations of the EOS, we improve the $T > 0$ results by taking account of possible shell effects in the entropy, which will manifest themselves in the free energy through the relation

$$f = e - Ts \quad , \quad (1.5)$$

where e is the energy per nucleon.

A further development of considerable significance is that the TETFSI method, as we shall refer to this temperature-dependent ETFSI method, is no longer limited to forces whose effective nucleon mass M^* is equal to the real mass M . This permits us to use more realistic effective forces with smaller values of the effective mass. Thus in the present calculations the effective interaction that we use is the Skyrme force BSk14, for which the effective mass in symmetric INM at the equilibrium density ρ_0 (0.159 nucleons.fm⁻³) is $0.800M$, which is to be compared with the value of $0.825M$ found in extended Brueckner-Hartree-Fock calculations that include three-nucleon forces [40]. This is the force that underlies

the Hartree-Fock-Bogoliubov (HFB) mass model HFB-14 [17], a force that is eminently suitable for calculating the properties of neutron-star crustal matter, since on the one hand it has been fitted to the properties of neutron matter, as determined by calculations with realistic two- and three-nucleon forces [41], and on the other hand it gives an excellent fit to essentially all the available mass data ($\sigma_{rms} = 0.729$ MeV). Given that the neutron-star crust is both inhomogeneous and contains some protons, the high quality of the mass fit is especially relevant, since it means a) that inhomogeneities in nuclear matter (surface effects in droplet-model language) are well modeled, and b) that neutron-proton interactions are well represented. (However, no Skyrme force should be used for the highly supernuclear densities encountered deep within the core of a neutron star.) We stress that in this paper we neglect pairing, as in Refs. [25, 26].

In Section II we discuss our parametrization of the WS cell. Section III describes our adaptation of the ETFSI method to the problem of the EOS of the neutron-star inner crust at non-zero temperatures, with particular attention to the convergence properties of the ETF expansion of the entropy. Our formalism is applied in Section IV to the properties of the inner crust of a neutron star (we do not examine in this paper the important question of the rapid decompression of neutron-star matter). The existence of strong proton-shell effects in the inner crust is discussed in this same section. Our conclusions are summarized in Section V. Some important material is to be found in the appendices, notably the TETF expansion of the specific heat (App. A) and a proof of the Strutinsky-integral theorem (App. C).

II. THE WIGNER-SEITZ CELL

Since we do not consider depths greater than that for which the mean density is $\bar{\rho} = 0.06$ nucleons.fm⁻³ only the droplet phase of nucleons has to be considered, and we shall assume that the WS cell associated with this phase is spherical, radius R_c . This cell is entirely representative of the macroscopically sized volume element being considered, in the sense that all the nucleons of this volume element are imagined to be grouped into identical such cells, there being one cell for each droplet. The average neutron and proton densities over the locally representative cell must thus each be equal to the local values of the corresponding

macroscopic densities, $\bar{\rho}_n$ and $\bar{\rho}_p$, given respectively by

$$\bar{\rho}_n = \bar{\rho}(1 - Y_e) \quad (2.1a)$$

and

$$\bar{\rho}_p = \bar{\rho}Y_e \quad , \quad (2.1b)$$

where Y_e is the fraction of nucleons that are protons. The neutron and proton density distribution functions within the cell, $\rho_n(\mathbf{r})$ and $\rho_p(\mathbf{r})$, are then constrained by

$$\frac{\int_{cell} \rho_q(\mathbf{r}) d^3\mathbf{r}}{\int_{cell} d^3\mathbf{r}} = \bar{\rho}_q = \frac{3}{R_c^3} \int_0^{R_c} \rho_q(r) r^2 dr \quad , \quad (2.2)$$

where q denotes n or p , as the case may be, and the second equality holds in the case of spherical symmetry, assumed here. The total number of nucleons of each type in the cell is

$$N_q = \frac{4\pi}{3} R_c^3 \bar{\rho}_q \quad (2.3)$$

($N_n = N$, $N_p = Z$).

For the neutron and proton density distribution functions we adopt a modified version of the simple Fermi form that we used in Ref. [1]: limiting ourselves to the spherical case and writing

$$\rho_q(r) = \rho_{Bq} + \rho_{0q} f_q(r) \quad , \quad (2.4)$$

in which ρ_{Bq} is the usual constant background term, we now take

$$f_q(r) = \frac{1}{1 + \frac{1}{e} \exp\left(\frac{C_q - R_c}{r - R_c}\right)^2 \exp\left(\frac{r - C_q}{a_q}\right)} \quad . \quad (2.5)$$

Here the denominator of the radially varying term contains an extra factor $\frac{1}{e} \exp\left(\frac{C_q - R_c}{r - R_c}\right)^2$, the presence of which guarantees that the density gradient now vanishes at the surface of the cell, thereby ensuring that the droplets merge smoothly with the homogeneous neutron vapor within the WS cell (in addition to being physically realistic, this condition is also required for the validity of the semi-classical part of the TETFSI method used here to calculate the nuclear kinetic energy and entropy). Also, again because of the extra factor, $f_q(r)$ itself vanishes on the surface of the WS cell, whence

$$\rho_q(R_c) = \rho_{Bq} \quad . \quad (2.6)$$

The factor $1/e$ ensures that the radially varying factor takes the value $\rho_{0q}/2$ at $r = C_q$, as usual. Finally, we note that $f_q(r)$ varies monotonically *over the cell*.

The two background constants ρ_{Bq} are not independent of the other parameters, but rather are fixed by

$$\rho_{Bq} = \bar{\rho}_q - \frac{3}{R_c^3} I_q \rho_{0q} \quad , \quad (2.7)$$

where

$$I_q = \int_0^{R_c} f_q(r) r^2 dr \quad . \quad (2.8)$$

For given $\bar{\rho}$ the WS cell is thus characterized by seven geometrical parameters, ρ_{0q} , C_q , a_q ($q = n, p$), and R_c , in addition to the composition parameter Y_e . In the most general case all eight of these parameters correspond to degrees of freedom, but either or both of the last two might be constrained to fixed values, according to the physical situation being described. In particular, for specified Z and N , the given value of $\bar{\rho}$ determines R_c .

But in all cases the complete set of parameters is subject to the additional constraint that the densities $\rho_q(r)$ must be positive at all points in the cell. We handle this problem as described in Section II of Ref. [1], the modified radial distribution leading to the simplified condition

$$\frac{\bar{\rho}_q}{(3I_q/R_c^3) - f_q(r=0)} < \rho_{0q} < \frac{R_c^3 \bar{\rho}_q}{3I_q} \quad , \quad (2.9)$$

given that $f_q(r)$ varies monotonically over the cell. The lower limit is seen from the mean-value theorem to be essentially negative, and since negative values of ρ_{0q} correspond to bubbles we shall be interested here only in the restricted range

$$0 < \rho_{0q} < \frac{R_c^3 \bar{\rho}_q}{3I_q} \quad . \quad (2.10)$$

Although this is of no concern for the present paper, it is convenient to note here that once decompression and beta decay have begun, it will be necessary to constrain the background parameters ρ_{Bq} to given values, since different (Z, A) configurations will be present simultaneously. Thus, with Eq. (2.7) still holding, the two degrees of freedom corresponding to the parameters ρ_{0q} will be lost. Rather, they will be determined uniquely according to

$$\rho_{0q} = \frac{R_c^3}{3I_q} (\bar{\rho}_q - \rho_{Bq}) \quad , \quad (2.11)$$

positive values still corresponding to droplets and negative to bubbles. The condition that the densities be everywhere positive then leads to constraints on the range of values that are possible for ρ_{Bq} :

$$0 < \rho_{Bq} < \frac{\bar{\rho}_q}{1 - 3I_q/\{R_c^3 f_q(r=0)\}} \quad , \quad (2.12)$$

in which the upper limit is essentially larger than $\bar{\rho}_q$, but only the restricted range

$$0 < \rho_{Bq} < \bar{\rho}_q \quad (2.13)$$

corresponds to droplets.

III. THE TETFSI METHOD

For a given set of the geometrical cell parameters we first write the total density of the Helmholtz free energy at a given point in the cell as

$$\mathcal{F}' = \mathcal{F}_{nuc} + \mathcal{F}_e + \mathcal{E}_c + (\bar{\rho}_n M_n + \bar{\rho}_p M_p + n_e m) c^2 \quad , \quad (3.1)$$

where \mathcal{F}_{nuc} is the specifically nuclear free-energy density (discussed below), \mathcal{F}_e is the density of the electron free energy (calculated essentially exactly), and \mathcal{E}_c is the Coulomb energy. (Strictly speaking, in this equation $\bar{\rho}_n$ and $\bar{\rho}_p$ should be replaced by ρ_n and ρ_p , respectively, but the differences vanish on integrating over the cell.) Since $\bar{\rho}_p = n_e$, electrical neutrality holding globally over the WS cell, we can now write

$$(\bar{\rho}_n M_n + \bar{\rho}_p M_p + n_e m) c^2 = \bar{\rho} \left\{ (1 - Y_e) M_n + Y_e (M_p + m) \right\} c^2 = \bar{\rho} M_n c^2 - \bar{\rho} Y_e Q_{n,\beta} \quad , \quad (3.2)$$

where $Q_{n,\beta}$ is the beta-decay energy of the neutron (0.782 MeV). But the term $\bar{\rho} M_n c^2$ makes a constant contribution to the free energy per nucleon and can thus be discarded. Thus in place of Eq. (3.1) we write

$$\mathcal{F} = \mathcal{F}_{nuc} + \mathcal{F}_e + \mathcal{E}_c - \bar{\rho} Y_e Q_{n,\beta} \quad . \quad (3.3)$$

The total Coulomb energy density, direct and exchange, is given in general by

$$\mathcal{E}_c(\mathbf{r}) = \frac{e^2}{2} \{ \rho_p(\mathbf{r}) - n_e \} \int \frac{\rho_p(\mathbf{r}') - n_e}{|\mathbf{r} - \mathbf{r}'|} d^3 \mathbf{r}' - \frac{3e^2}{4} \left(\frac{3}{\pi} \right)^{1/3} (\rho_p^{4/3} + n_e^{4/3}) \quad , \quad (3.4)$$

where for the exchange term we have used the usual Kohn-Sham variant [42] of the Slater approximation. The last equation reduces in the case of spherical symmetry to

$$\mathcal{E}_c = 2\pi e^2(\rho_p - n_e) \left\{ \int_0^r \rho_p(r') \left(\frac{r'^2}{r} - r' \right) dr' + n_e \frac{r^2}{6} \right\} - \frac{3e^2}{4} \left(\frac{3}{\pi} \right)^{1/3} (\rho_p^{4/3} + n_e^{4/3}) \quad . \quad (3.5)$$

The mean free energy per nucleon in the entire system is given by the corresponding quantity averaged over just one cell,

$$f = \frac{1}{A} \int \mathcal{F}(\mathbf{r}) d^3\mathbf{r} \quad , \quad (3.6)$$

where $A = N + Z$ is the total number of nucleons in the cell. We shall likewise calculate the total entropy, the density of which at a given point can be written as

$$\sigma = \sigma_{nuc} + \sigma_e = \sigma_n + \sigma_p + \sigma_e \quad , \quad (3.7)$$

whence for the mean total entropy per nucleon we have

$$s = \frac{1}{A} \int \sigma(\mathbf{r}) d^3\mathbf{r} \quad . \quad (3.8)$$

The Skyrme force BSk14 [17] for which we calculate the densities \mathcal{F}_{nuc} and σ_{nuc} has the usual form

$$\begin{aligned} v_{ij} = & t_0(1 + x_0 P_\sigma) \delta(\mathbf{r}_{ij}) + t_1(1 + x_1 P_\sigma) \frac{1}{2\hbar^2} \{ p_{ij}^2 \delta(\mathbf{r}_{ij}) + h.c. \} \\ & + t_2(1 + x_2 P_\sigma) \frac{1}{\hbar^2} \mathbf{p}_{ij} \cdot \delta(\mathbf{r}_{ij}) \mathbf{p}_{ij} + \frac{1}{6} t_3(1 + x_3 P_\sigma) \rho^\alpha \delta(\mathbf{r}_{ij}) \\ & + \frac{i}{\hbar^2} W_0(\boldsymbol{\sigma}_i + \boldsymbol{\sigma}_j) \cdot \mathbf{p}_{ij} \times \delta(\mathbf{r}_{ij}) \mathbf{p}_{ij} \quad . \end{aligned} \quad (3.9)$$

The total nuclear energy density at any point can now be written as

$$\mathcal{E}_{nuc} = \sum_q \left(\frac{\hbar^2}{2M_q^*} \tau_q \right) + \mathcal{V} \quad , \quad (3.10)$$

where τ_q gives the kinetic-energy density of nucleons q as $\frac{\hbar^2}{2M_q} \tau_q$ (the first term of Eq. (3.10) is the kinetic-energy density multiplied by M_q/M_q^*), the effective mass M_q^* is given by

$$\begin{aligned} \frac{\hbar^2}{2M_q^*} = & \frac{\hbar^2}{2M_q} + \frac{1}{8} \left\{ t_1(2 + x_1) + t_2(2 + x_2) \right\} \rho \\ & + \frac{1}{8} \left\{ t_2(1 + 2x_2) - t_1(1 + 2x_1) \right\} \rho_q \quad , \end{aligned} \quad (3.11)$$

and the static part of the potential energy by

$$\begin{aligned}
\mathcal{V} = & \frac{1}{4}t_0\left\{(2+x_0)\rho^2 - (1+2x_0)\sum_q\rho_q^2\right\} \\
& + \frac{1}{32}\left\{3t_1(2+x_1) - t_2(2+x_2)\right\}(\nabla\rho)^2 \\
& - \frac{1}{32}\left\{3t_1(1+2x_1) + t_2(1+2x_2)\right\}\sum_q(\nabla\rho_q)^2 \\
& + \frac{1}{24}t_3\left\{(2+x_3)\rho^2 - (1+2x_3)\sum_q\rho_q^2\right\}\rho^\alpha \\
& + \frac{1}{2}W_0\sum_q\mathbf{J}_q\cdot\nabla(\rho+\rho_q) \quad , \tag{3.12}
\end{aligned}$$

in which \mathbf{J}_q is the spin-current density, and we have now set the “quadratic current” term \mathcal{V}_{JJ} of Eq. (A4c) of Ref. [1] equal to 0 throughout the calculation (our treatment of this term in Ref. [1] was inconsistent). For the nuclear free-energy density at any point we then have

$$\mathcal{F}_{nuc} = \sum_q \mathcal{K}_q + \mathcal{V} \quad , \tag{3.13}$$

where

$$\mathcal{K}_q = \frac{\hbar^2}{2M_q^*}\tau_q - T\sigma_q \quad . \tag{3.14}$$

The first stage of the full TETFSI method that we adopt in this paper for a given temperature T , mean density $\bar{\rho}$ and fixed values of N and Z consists in approximating the exact HF value of the nuclear free-energy density \mathcal{F}_{nuc} for the given Skyrme force by the full fourth-order TETF method of BBD [43]: see, for example, our paper [1], the appendix of which contains a convenient summary of the formalism, as we have used it here. We do not repeat this formalism here, although in Appendix A we present the TETF expansion for the specific heat, which appears not to have previously been published. Moreover, we remark here that the TETF expression for σ_q given by BBD [43] assumes that

$$\sigma = -\left(\frac{\partial\mathcal{F}}{\partial T}\right)_{\rho,X} \quad , \tag{3.15}$$

where it is to be noted that it is the local density ρ , and not the mean density $\bar{\rho}$, that is held constant. We show in Appendix B that Eq. (3.15) follows from Eq. (1.4) only if

equilibrium holds (this condition is made necessary by virtue of the temperature dependence of the density distribution itself).

The essence of the TETF method is to express τ_q , \mathbf{J}_q and σ_q in terms of an assumed density distribution, which here we take to have the form given in Eqns. (2.4) and (2.5). The value that we obtain for the total free energy per nucleon f , as given by Eqns. (3.3) and (3.6), is minimized with respect to the six geometrical parameters ρ_{0q} , C_q , a_q of the parametrized nucleon distribution. (In looking for full nuclear and beta equilibrium we minimize with respect to N and Z also.) The resulting nucleon distributions are denoted by $\tilde{\rho}_q$, and the corresponding approximations to τ_q , \mathbf{J}_q , σ_q and f by $\tilde{\tau}_q$, $\tilde{\mathbf{J}}_q$, $\tilde{\sigma}_q$ and f_{TETF} respectively. The value of all these approximations to the exact HF values vary smoothly with respect to N and Z : it is a characteristic of the TETF method that shell corrections are lost. In the second stage we use the Strutinsky-integral method to correct f_{TETF} perturbatively for proton shell effects, as follows.

At zero temperature, where $f_{TETF} = e_{ETF}$, the corrected value of e takes the form

$$e = e_{ETF} + \frac{1}{A} E_p^{sc} \quad , \quad (3.16)$$

where, according to the Strutinsky-integral theorem,

$$E_p^{sc} = \sum_i n_i \tilde{\epsilon}_{i,p} - \int d^3\mathbf{r} \left(\frac{\hbar^2}{2M_p^*} \tilde{\tau}_p + \tilde{\rho}_p \tilde{U}_p + \tilde{\mathbf{J}}_p \cdot \widetilde{\mathbf{W}}_p \right) \quad . \quad (3.17)$$

Here the integral goes over the volume of the WS cell, while the sum goes over all the occupied s.p. proton states, with the s.p. energies $\tilde{\epsilon}_{i,p}$ being the eigenvalues of the s.p. Schrödinger equation

$$\left\{ -\nabla \frac{\hbar^2}{2M_p^*(\mathbf{r})} \cdot \nabla + \tilde{U}_p(\mathbf{r}) - i \widetilde{\mathbf{W}}_p(\mathbf{r}) \cdot \nabla \times \boldsymbol{\sigma} \right\} \phi_{i,p} = \tilde{\epsilon}_{i,p} \phi_{i,p} \quad , \quad (3.18)$$

and n_i the occupancy of s.p. state i ($= 0$ or 1 for $T = 0$ and no pairing). In these last two equations the effective mass \widetilde{M}_p^* is given by Eq. (3.11) with the smooth ETF densities $\tilde{\rho}_q$ replacing the exact HF densities ρ_q . Likewise \tilde{U}_p and $\widetilde{\mathbf{W}}_p$ are the central and spin-orbit proton fields, respectively, given by the usual HF expressions for these fields (see, for example, Eqns. (7) and (9) of Ref. [44]), with $\tilde{\rho}_q$ replacing ρ_q (note that here \tilde{U}_p contains the Coulomb field).

All three of these fields involve a folding of the Skyrme force over the nucleon distribution $\tilde{\rho}_q$ that emerges from the minimisation of e_{ETF} in the ETF part of the calculation. The fact

that the same Skyrme force underlies also the ETF part of the calculation implies a high degree of consistency between the two parts, which probably accounts for the close agreement found in comparisons with exact self-consistent HF calculations [34, 35] (note that these tests were limited to the case of bound nuclei at $T = 0$ and with $M_q^* = M_q$). This theorem seems to have been stated for the first time in Ref. [45]. A derivation, limited, however, to the case $M_q^* = M_q$, was sketched in Ref. [38]. A more complete proof, applicable to arbitrary effective mass, is presented in Appendix C.

As for $T > 0$, in Ref. [39] we replaced Eq. (3.16) by

$$f = f_{ETF} + \frac{1}{A} E_p^{sc} \quad , \quad (3.19)$$

where the proton shell correction is still given by Eq. (3.17), with

$$n_i = \frac{1}{1 + \exp\{(\widetilde{\epsilon}_{i,p} - \mu_p)/T\}} \quad , \quad (3.20)$$

μ_p being the chemical potential for protons. However, this does not take account of possible proton shell effects in the entropy, so here we will write rather

$$f_{ETF\text{SI}} = f_{ETF} + \frac{1}{A} E_p^{sc} - T(s_p^{s.p.} - s_p^{ETF}) \quad , \quad (3.21)$$

where $s_p^{s.p.}$ is the usual s.p. expression for the proton entropy,

$$s_p^{s.p.} = - \sum_i \{n_i \ln n_i + (1 - n_i) \ln (1 - n_i)\} \quad , \quad (3.22)$$

in which the sum goes over all proton states.

To determine the eigenvalues $\widetilde{\epsilon}_{i,p}$ we expand the eigensolutions $\phi_{i,p}$ to Eq. (3.18) in the basis defined by spherical Bessel functions $j_l(k_n r)$ with the k_n chosen to satisfy homogeneous boundary conditions (vanishing of the function or of its first derivative) on the surface of the WS cell. This generates a complete set of functions that are orthogonal over the cell, and we diagonalize the associated matrix.

Interpolation Schemes. In addition to its much greater simplicity and rapidity, as compared to full-blown HF calculations, the (T)ETF\text{SI} method has the advantage of lending itself to interpolation. The point is that while the shell corrections are indeed fluctuating quantities, the method expresses these quantities in terms of quantities that themselves vary smoothly: the fluctuations arise entirely in the summation indicated on the right-hand side of Eq. (3.17). This feature was heavily exploited in the construction of the ETF\text{SI}-1 mass

table, the first mass table to be based on microscopic forces [38], and we anticipate that it could prove equally fruitful for the extensive tabulation of the EOS described in this paper.

Specific heat. It is convenient to define a density of specific heat at constant volume, $\mathcal{C}_v(\mathbf{r})$, at each point in the cell, according to

$$c_v = \frac{1}{A} \int \mathcal{C}_v(\mathbf{r}) d^3\mathbf{r} \quad , \quad (3.23)$$

where c_v is the specific heat per nucleon (1.3), and the integration goes over the volume of the WS cell. It then follows, provided equilibrium holds, that

$$\mathcal{C}_v(\mathbf{r}) = T \left(\frac{\partial \sigma}{\partial T} \right)_{\rho, X} \quad (3.24)$$

(see Appendix B). This last result can then be used, starting from the TETF expansion of σ [43], to derive the corresponding expansion for \mathcal{C}_v up to order \hbar^4 . This expansion is presented in Appendix A.

Convergence of the TETF expansions.

Before applying the TETFSI method to the calculation of the neutron-star crust we make extensive tests of the convergence of the series expansion implicit in the TETF method. For this it is convenient to define the quantity

$$\phi_q = \frac{4\pi}{A} \int_0^{R_c} \mathcal{K}_q(r) r^2 dr \quad , \quad (3.25)$$

which is just the “kinetic-thermal” part of the nuclear free energy per nucleon.

We consider two densities, $\bar{\rho} = 0.06$ and 3×10^{-4} nucleons.fm $^{-3}$, which lie close to the upper and lower limits, respectively, of the density range encountered in the inner crust. For the former we take a cell with $Z = 30$, $A = 1123$, and for the latter $Z = 40$, $A = 150$, these lying close to the equilibrium configuration (see Section IV). The results are shown in Tables I and II, respectively, for three temperatures, 0.1, 1.0, and 3.0 MeV. For each quantity, ϕ_n and ϕ_p , we show in successive lines the Thomas-Fermi (TF) approximation, the second-order correction in \hbar , and the fourth-order correction; the sum of these three contributions is shown in the adjacent column. We also show in these tables the corresponding expansion terms for s_n , s_p , $c_{v,n}$, $c_{v,p}$ and the proton entropy as calculated by the s.p. expression (3.22).

We see that the expansions for all the neutron quantities, ϕ_n , ϕ_p , s_n , and $c_{v,n}$, converge well over the entire density and temperature range. However, the expansions for the proton entropy s_p and the related specific heat $c_{v,p}$ diverge badly at low temperature, to the point of

occasionally giving negative entropies and specific heats. This proton-related problem is seen to be worse at low densities, which suggests that the fact that the neutron-related quantities converge so much better might be related to the fact that our neutron densities are always much higher than the proton densities. Indeed, we find that at an outer-crust density of $\bar{\rho} = 1 \times 10^{-4} \text{ nucleons.fm}^{-3}$ the TETF expansion for the neutron entropy of ^{208}Pb converges rather poorly. The existence of a significant background term, which gives no contribution to either the second- or fourth-order terms, appears to be crucial in this respect. It is fortunate that the lower density limit for good convergence of the TETF expansion for the neutron entropy lies below our domain of interest. In any case, it is quite clear that we cannot use the TETF expansions for the proton entropy or specific heat.

For the proton entropy we therefore fall back instead on the s.p. expression (3.22), which we require anyway for the proton shell corrections. On the other hand, we recall that we cannot use this s.p. expression for the neutron entropy because of continuum problems: it was precisely for this reason that we had to abandon the HF approach. As for the proton specific heat, we could in principle calculate numerically the temperature derivative of the proton entropy (3.22) and use Eq. (1.3), but this is too time-consuming, if done accurately. We thus simply take the TF approximation for the proton contribution to the specific heat. Since the neutron contribution dominates the specific heat, the error thereby introduced will be relatively small; in any case we see that at higher temperatures the TF approximation to the entropy agrees approximately with the entropy calculated by Eq. (3.22).

It is reasonable to ask why the TETF entropy expansion diverges at low T . The second-order term contains a T^{-1} factor, and the fourth-order term a T^{-2} factor (see Eqns. (A.25b-c) of Ref. [1]), so that the corresponding numerators must likewise vanish at low T . This suggests that a massive cancellation within these numerators is leading to a significant loss of precision. However, we derived the low- T (strong degeneracy) limit of the TETF entropy expansion (see Appendix D), and found essentially the same numerical results. We suggest that the reason for the observed breakdown in the TETF expansions of the entropy and specific heat lies with the fact that the validity of Eqns. (3.15) and (3.24) requires that the system be in equilibrium, which can never be exactly the case when the density profiles are parametrized, as in Eqns. (2.4) and (2.5).

IV. EQUILIBRIUM PROPERTIES OF INNER CRUST

Pure TETF calculations. In calculating the equilibrium (nuclear and beta) composition of the inner crust, i.e., the number Z of protons and the number N of neutrons per WS cell at any given mean density $\bar{\rho}$, we shall first neglect shell corrections. For this we simply minimize f_{TETF} , calculated at $T = 0$, with respect to N and Z . The results for Z , $A = Z + N$, and $Y_e = Z/A$ are shown in Figs. 1, 2, and 3, respectively. We stress that in this picture Z and A vary continuously, and are not restricted to integral values.

These figures also show the values of the same quantities that we find for the force SLy4 [46], which has been widely applied to neutron stars. Fig. 2 for A shows that at a given $\bar{\rho}$ the WS cells tend to be bigger for force BSk14, presumably because the value of the surface-energy coefficient a_{sf} is slightly larger for the former (18.11 MeV as opposed to 17.6 MeV). However, since Y_e runs slightly higher for SLy4 (see Fig. 3) there are generally somewhat more protons for this latter force, as seen in Fig. 1. (The higher values of Y_e found for SLy4 can be traced to the fact that in homogeneous neutron matter the energy per neutron is higher for SLy4 over the entire density range considered here.) This sensitivity to the choice of force will have implications both for transport properties in the inner crust and for nucleosynthesis in decompressing neutron-star matter.

Now the popular EOS of Ref. [47] is also based on the SLy4 force, to the extent that the parameters of the underlying compressible liquid-drop model are calculated for this force. We compare the results of Ref. [47] for Z with our own in Fig. 4, where it will be seen that the two models lead to appreciable differences even before taking shell effects into account.

TETFSI calculations: proton shell effects. When shell corrections are included Z and A must be considered as integers, and thus change discontinuously: each (Z, A) pair defines a phase. Since $\bar{\rho}$ changes continuously transitions between one phase and another will take place over a finite range of $\bar{\rho}$, in which the two phases coexist. We shall neglect this feature (see, however, the comments below), but our results will be valid over those considerable intervals of $\bar{\rho}$ for which only a single phase exists.

The calculations proceed as outlined in Section III. Thus for given values of T and $\bar{\rho}$, and for a given (Z, A) pair, f_{TETF} has to be minimized with respect to the geometrical parameters of the cell, and then shell-corrected according to Eq. (3.19) (note that the (T)ETFSI method calculates shell corrections perturbatively). The equilibrium values of Z

and A , i.e., the values that minimize the TETFSI value of f for given values of T and $\bar{\rho}$, are shown as functions of $\bar{\rho}$ for $T = 0, 0.1$, and 1.0 MeV in Tables III, IV, and V, respectively.

With the TETF values being shown in parentheses, we see in Tables III and IV that at $T = 0$ and 0.1 MeV there are strong proton shell effects, with $Z = 50, 40$, and 20 being successively favored as the density increases; in fact, these are the *only* values of Z that appear. The changes from $Z = 50$ at $\bar{\rho} = 0.005 \text{ fm}^{-3}$ to $Z = 40$ at 0.01 fm^{-3} and from $Z = 40$ at $\bar{\rho} = 0.04 \text{ fm}^{-3}$ to $Z = 20$ at 0.05 fm^{-3} appear to be discontinuous. This situation can easily be understood from Figs. 5 and 6, where we show f at $T = 0.1$ MeV as a function of Z for $\bar{\rho} = 0.005$ and 0.04 fm^{-3} , respectively, minimizing with respect to A for each value of Z : relatively strong minima occur for $Z = 50, 40$ and 20 , and the system flips from one to the next as the density increases. (Somewhat surprisingly, although $Z = 28$ is consistently a strong local minimum it is never an absolute minimum.) It is noteworthy that the value of $Z = 50$ that we find here at the outside edge of the inner crust agrees with what we find for an *outer*-crust calculation using the HFB-14 mass model [17], i.e., a mass model based on the BSk14 force used here.

It will be seen from Figs. 5 and 6 that the minima are very close in energy, and numerical uncertainties in our computation often make it impossible to affirm with certainty which magic number prevails at a given density. Certainly, changing the force could be expected to lead to changes in the sequence of magic numbers. In fact, Negele and Vautherin [26] report a quite different sequence for the proton numbers 40 and 50 (and do not find $Z = 20$ at any density). At $T = 0.1$ MeV the energy fluctuations associated with the Boltzmann factor represent an uncertainty on the total cell energy, and thus amount to $0.1/A$ MeV per nucleon. Reference to Figs. 5 and 6 then shows that there will be negligible admixture of other values of Z with the magic values, although there could be significant admixture of A -values.

Tables III and IV reveal no essential difference between $T = 0$ and $T = 0.1$ MeV. However, with the energy differences between adjacent magic numbers being so small it could be that there are some intermediate densities for which the composition changes as T varies between 0 and 0.1 MeV. This is one sense in which caution might have to be exercised in adopting the picture of “cold catalyzed matter”.

Table V shows that at $T = 1$ MeV shell effects have effectively been wiped out, even though there are still significant differences between the TETF and TETFSI values. This

raises the question of whether a nuclear equilibrium in the crust of a cooling neutron star can be maintained right down to $T = 0.1$ MeV. If “freeze-out” were to occur at, or slightly below, $T = 1$ MeV, i.e., if the complex rearrangement of nucleons necessary to maintain nuclear equilibrium could no longer take place over the lifetime of the neutron star, then the sharp shell effects that we have predicted here would not be observed. This is another, and probably more serious sense, in which the picture of “cold catalyzed matter” has to be carefully scrutinized.

Pressure. We extract P directly from the computed values of f_{TETFSI} using Eq. (1.2), numerically evaluating the derivative with a 3-point Savitzky-Golay filter (routine ‘savgol’ [48]). Our results are shown in the penultimate columns of Tables III, IV, and V; tests show that over this density range our results for P are reliable to within about 1 %.

Another quantity of astrophysical interest is the temperature variation of the pressure $\left(\frac{\partial P}{\partial T}\right)_{\bar{\rho}}$; using a well known Maxwell relation we have

$$\left(\frac{\partial P}{\partial T}\right)_{\bar{\rho}} = -\bar{\rho}^2 \left(\frac{\partial s}{\partial \bar{\rho}}\right)_T . \quad (4.1)$$

This too requires a numerical differentiation, but only one: without using the Maxwell relation we would have to perform *two* numerical differentiations, with consequent loss of precision. Moreover, the derivative of s can be computed simultaneously with the one of f that gives us P , with negligible increase in computer time. The results are shown in the last columns of Tables III, IV, and V.

Phase equilibrium. If we were to consider a quasi-continuum of values of $\bar{\rho}$ our calculations might show unphysical discontinuities in the pressure at the transition between the different (Z, A) phases. This is a result of our neglect of the possibility of a thermal equilibrium between the two phases in question, and in reality the pressure remains continuous. The transition pressure P is characterized by equality of the Gibbs free energy per nucleon in each phase,

$$g_1 = g_2 \quad , \quad (4.2)$$

where

$$g_i = f_i + \frac{P}{\bar{\rho}_i} . \quad (4.3)$$

We stress that the equilibrium pressure satisfying this condition can be determined by calculating f_i as a function of $\bar{\rho}$ for each phase separately; in particular it is at no point necessary

to minimize the Gibbs function itself. Moreover, it can be shown that the condition (4.2) follows from a minimization of the total *Helmholtz* function [49].

V. CONCLUSIONS

We have developed here a high-speed approximation to the HF method for calculating the EOS of the neutron-star inner crust with Skyrme-type forces. Our method, which we refer to as the TETFSI method, models the inner crust in terms of the Wigner-Seitz cell, and consists essentially of a generalization to finite temperatures (and arbitrary effective mass) of the ETFSI method originally developed as a mass model [34, 35, 36, 37, 38]. An essential difference between our TETFSI method and a full-scale HF calculation of the EOS is that, whereas the latter method inevitably and automatically calculates both neutron and proton shell effects, here we calculate only the latter, since in reality shell effects are much weaker for neutrons than for protons, and will have negligible impact on the composition. In fact, if the HF method is used in a WS picture, as in the classical work of Negele and Vautherin[26] it will lead, because of discretization, to spuriously large neutron shell effects[30]. As in Ref. [26], we have neglected pairing in this paper, pending the determination of an effective pairing interaction appropriate to the conditions pertaining in neutron-star crusts. Nevertheless, it will be easy to include pairing in the (T)ETFSI framework, as already done in the ETFSI mass models [34, 35, 36, 37, 38].

It was found that the TETF expansion of the entropy converges badly at low temperatures for densities typical of inner-crust protons (there was no problem for neutrons). We solved this difficulty by using the s.p. expression for the proton entropy.

Our exploratory calculations of the EOS were performed with the Skyrme-type force BSk14, a force that was fitted to essentially all the nuclear-mass data, forming thereby the basis of the HFB-14 mass model [17]. This force is particularly suitable for calculating the properties of neutron-star crustal matter, because it has been fitted to the properties of homogeneous neutron matter while at the same time the good fit to masses ensures that both inhomogeneities and the neutron-proton interaction are well represented.

The calculated composition of the WS cells representing the clustering in the inner crust showed striking shell effects: for $T = 0$ the proton number Z was limited to the magic values of 50, 40 and 20, the value decreasing with increasing density (at the interface with

the outer crust we found continuity with an outer-crust calculation based on the HFB-14 mass model). Although essentially identical results are obtained for $T = 0.1$ MeV, all our calculated shell effects are wiped out at $T = 1$ MeV, which means that whether or not shell effects actually exist in the cold crust depends very much on the “freeze-out” temperature for nuclear equilibrium. On the other hand, we have shown that even without taking shell effects into account there are considerable differences between our predictions and those of the compressible liquid-drop model on which the EOS of Ref. [47] is based.

We intend to apply the method described here to a study of the synthesis of r-process nuclei in decompressing neutron-star crustal matter. To this end we present here, apparently for the first time, the TETF expressions for the specific heat of an inhomogeneous system of nucleons. In this same context of extensive computations over a wide range of temperature, density and composition, we point out that the (T)ETFSI method lends itself admirably to interpolation, without any loss of precision in the calculated shell effects, essentially because these arise in the sums of quantities that themselves vary smoothly [36].

Acknowledgments

We are indebted to B. K. Jennings for suggesting to us the Strutinsky-integral method. M. Brack and J. M. Lattimer are thanked for stimulating discussions in the early stages of this work. The financial support of the NSERC (Canada) and the FNRS (Belgium) is acknowledged. N.C. gratefully acknowledges the award of a Marie Curie Intra-European fellowship (contract number MEIF-CT-2005-024660).

APPENDIX A: TETF EXPRESSIONS FOR THE SPECIFIC-HEAT DENSITY \mathcal{C}_v

We expand the specific-heat density \mathcal{C}_v of Eq. (3.24) according to

$$\mathcal{C}_v = \mathcal{C}_v^{(TF)} + \mathcal{C}_v^{(2)} + \mathcal{C}_v^{(4)} + \dots \quad , \quad (\text{A.1})$$

where the first term on the right-hand side represents the Thomas-Fermi approximation, the second term the first-order correction in \hbar^2 , and the last term the second-order correction

in \hbar^2 . Then

$$\mathcal{C}_{v,q}^{(TF)} = \frac{3}{2} \left\{ \sigma_q^{(TF)} + \eta_q \rho_q - 3\rho_q \frac{I_{1/2}(\eta_q)}{I_{-1/2}(\eta_q)} \right\} \quad (\text{A.2a})$$

$$\mathcal{C}_{v,q}^{(2)} = -\frac{\sigma_q^{(2)}}{16\nu_q} (24x^3 + 22x^2 + 5x - 63xy - 33y + 45z) \quad (\text{A.2b})$$

$$\mathcal{C}_{v,q}^{(4)} = -2\sigma_q^{(4)} - 3 \left(\frac{\hbar^2}{2MT} \right)^2 \frac{I_{1/2}(\eta_q)}{I_{-1/2}(\eta_q)} \sum_{i=1,3} G_i^q \left(\frac{\partial \chi_i}{\partial \eta_q} \right)_T \quad (\text{A.2c})$$

In Eq. (A.2c) we have

$$G_1^q = \frac{(\nabla^2 \rho_q)^2}{\rho_q} \quad (\text{A.3a})$$

$$G_2^q = \frac{\nabla^2 \rho_q (\nabla \rho_q)^2}{\rho_q^2} \quad (\text{A.3b})$$

$$G_3^q = \frac{(\nabla \rho_q)^4}{\rho_q^3} \quad (\text{A.3c})$$

and

$$\begin{aligned} \left(\frac{\partial \chi_1}{\partial \eta_q} \right)_T &= \left\{ \frac{I_{-1/2}(\eta_q)}{I_{1/2}(\eta_q)} \right\}^2 \left(\frac{11}{192} x^3 - \frac{11}{60} xy - \frac{109}{320} x^2 y + \frac{5}{64} x^4 + \frac{25}{64} xz \right. \\ &\quad \left. + \frac{5}{576} x^2 + \frac{11}{64} z - \frac{1}{64} y + \frac{3}{20} y^2 - \frac{21}{64} w \right) \end{aligned} \quad (\text{A.4a})$$

$$\begin{aligned} \left(\frac{\partial \chi_2}{\partial \eta_q} \right)_T &= \left\{ \frac{I_{-1/2}(\eta_q)}{I_{1/2}(\eta_q)} \right\}^2 \left(\frac{85}{288} x^4 - \frac{119}{96} w + \frac{1}{6} z + \frac{187}{320} y^2 + \frac{1}{18} x^3 - \frac{161}{80} x^3 y \right. \\ &\quad \left. + \frac{609}{320} xy^2 - \frac{175}{64} xw + \frac{159}{64} x^2 z - \frac{117}{64} yz - \frac{629}{480} x^2 y - \frac{11}{60} xy + \frac{289}{192} xz \right. \\ &\quad \left. + \frac{35}{96} x^5 + \frac{63}{32} v \right) \end{aligned} \quad (\text{A.4b})$$

$$\begin{aligned} \left(\frac{\partial \chi_3}{\partial \eta_q} \right)_T &= \left\{ \frac{I_{-1/2}(\eta_q)}{I_{1/2}(\eta_q)} \right\}^2 \left(-\frac{77}{256} w + \frac{11}{192} x^4 + \frac{33}{256} y^2 - \frac{693}{256} u - \frac{391}{240} x^3 y + \frac{2047}{1280} xy^2 \right. \\ &\quad - \frac{719}{320} x^4 y - \frac{161}{64} xw + \frac{97}{32} x^3 z - \frac{63}{16} x^2 w + \frac{1071}{256} xv + \frac{69}{32} x^2 z \\ &\quad - \frac{207}{128} yz + \frac{315}{128} yw - \frac{11}{40} x^2 y + \frac{11}{32} xz + \frac{161}{576} x^5 + \frac{483}{256} v \\ &\quad \left. + \frac{21}{64} x^6 + \frac{4317}{1280} x^2 y^2 - \frac{645}{128} xyz - \frac{801}{1280} y^3 + \frac{135}{128} z^2 \right) . \end{aligned} \quad (\text{A.4c})$$

All quantities shown here are as defined in the Appendix of Ref. [1] and Appendix B of Ref. [43], except for u , which we define according to

$$u = \frac{(I_{1/2})^6 I_{-13/2}}{(I_{-1/2})^7} \quad . \quad (\text{A.5})$$

Note that Eq. (A.2c) for the fourth-order term is valid only for an effective mass $M_q^* = M_q$ (see the Appendix of Ref. [1]).

As is the usual practice in expositions of the TETF method [43], we have dropped terms here that vanish on integrating over configuration space, which in the present case corresponds to the WS cell. That is why we have required the density gradients to vanish at the surface of the cell (see Section II).

APPENDIX B: PROOF OF EQNS. (3.15) AND (3.24)

The total free energy of the WS cell can be written as

$$F = \int \mathcal{F}(\rho, \nabla \rho, T) d^3 \mathbf{r} \quad , \quad (\text{B.1})$$

where the integration goes over the volume of the cell. For the entropy of the cell we have

$$\begin{aligned} S &= -\left(\frac{\partial F}{\partial T}\right)_{\bar{\rho}} = -\int \left(\frac{\partial \mathcal{F}}{\partial T}\right)_{\bar{\rho}} d^3 \mathbf{r} \\ &= -\int \left\{ \left(\frac{\partial \mathcal{F}}{\partial T}\right)_{\rho} + \left(\frac{\partial \mathcal{F}}{\partial \rho}\right)_T \left(\frac{\partial \rho}{\partial T}\right)_{\bar{\rho}} + \left(\frac{\partial \mathcal{F}}{\partial \nabla \rho}\right)_T \cdot \left(\frac{\partial \nabla \rho}{\partial T}\right)_{\bar{\rho}} \right\} d^3 \mathbf{r} \quad . \end{aligned} \quad (\text{B.2})$$

But, integrating by parts, we have

$$\begin{aligned} \int \left(\frac{\partial \mathcal{F}}{\partial \nabla \rho}\right)_T \cdot \left(\frac{\partial \nabla \rho}{\partial T}\right)_{\bar{\rho}} d^3 \mathbf{r} &= \int \left(\frac{\partial \mathcal{F}}{\partial \nabla \rho}\right)_T \cdot \nabla \left(\frac{\partial \rho}{\partial T}\right)_{\bar{\rho}} d^3 \mathbf{r} \\ &= -\int \left(\frac{\partial \rho}{\partial T}\right)_{\bar{\rho}} \nabla \cdot \left(\frac{\partial \mathcal{F}}{\partial \nabla \rho}\right)_T d^3 \mathbf{r} \quad , \end{aligned} \quad (\text{B.3})$$

where we are making use of the vanishing of $(\partial \mathcal{F} / \partial \nabla \rho)_T$ on the surface of the cell; this follows from the fact that \mathcal{F} must be at least quadratic in $\nabla \rho$, which must vanish on the surface of the cell for the TETF formalism to be valid. Then Eq. (B.2) becomes

$$-S = \int \left(\frac{\partial \mathcal{F}}{\partial T}\right)_{\rho} d^3 \mathbf{r} + \int \left(\frac{\partial \rho}{\partial T}\right)_{\bar{\rho}} \left\{ \left(\frac{\partial \mathcal{F}}{\partial \rho}\right)_T - \nabla \cdot \left(\frac{\partial \mathcal{F}}{\partial \nabla \rho}\right)_T \right\} d^3 \mathbf{r} \quad . \quad (\text{B.4})$$

Now if equilibrium holds at each temperature F must be a minimum with respect to variations in $\rho(\mathbf{r})$, which must therefore satisfy the Euler-Lagrange equation,

$$\left(\frac{\partial \mathcal{F}}{\partial \rho}\right)_T - \nabla \cdot \left(\frac{\partial \mathcal{F}}{\partial \nabla \rho}\right)_T = \lambda \quad , \quad (\text{B.5})$$

where λ is a Lagrange multiplier. Thus Eq. (B.4) becomes

$$-S = \int \left(\frac{\partial \mathcal{F}}{\partial T}\right)_\rho d^3\mathbf{r} + \lambda \int \left(\frac{\partial \rho}{\partial T}\right)_{\bar{\rho}} d^3\mathbf{r} = \int \left(\frac{\partial \mathcal{F}}{\partial T}\right)_\rho d^3\mathbf{r} + \lambda \left(\frac{\partial}{\partial T}\right)_{\bar{\rho}} \int \rho d^3\mathbf{r} \quad . \quad (\text{B.6})$$

But the second integral here is just the total number of nucleons in the cell (for simplicity we consider just one type of nucleon here), and since this is temperature independent Eq. (B.6) reduces to

$$S = - \int \left(\frac{\partial \mathcal{F}}{\partial T}\right)_\rho d^3\mathbf{r} \quad . \quad (\text{B.7})$$

Eq. (3.15) follows at once.

Likewise, for the specific heat we have from Eqns. (1.3) and (3.21)

$$Ac_v = T \left(\frac{\partial S}{\partial T}\right)_{\bar{\rho}} = T \int \left(\frac{\partial \sigma}{\partial T}\right)_{\bar{\rho}} d^3\mathbf{r} \quad . \quad (\text{B.8})$$

Then in exactly the same way as we have derived Eq. (B.4), we find

$$Ac_v = T \int \left(\frac{\partial \sigma}{\partial T}\right)_\rho d^3\mathbf{r} + T \int \left(\frac{\partial \rho}{\partial T}\right)_{\bar{\rho}} \left\{ \left(\frac{\partial \sigma}{\partial \rho}\right)_T - \nabla \cdot \left(\frac{\partial \sigma}{\partial \nabla \rho}\right)_T \right\} d^3\mathbf{r} \quad . \quad (\text{B.9})$$

In the second term here we can write, using Eq. (3.15),

$$\begin{aligned} \left(\frac{\partial \sigma}{\partial \rho}\right)_T - \nabla \cdot \left(\frac{\partial \sigma}{\partial \nabla \rho}\right)_T = \\ - \left(\frac{\partial}{\partial T}\right)_\rho \left\{ \left(\frac{\partial \mathcal{F}}{\partial \rho}\right)_T - \nabla \cdot \left(\frac{\partial \mathcal{F}}{\partial \nabla \rho}\right)_T \right\} \quad . \end{aligned} \quad (\text{B.10})$$

But if we are at equilibrium Eq. (B.5) will hold, and both sides of Eq. (B.10) will vanish, whence Eq. (B.9) reduces to

$$Ac_v = T \int \left(\frac{\partial \sigma}{\partial T}\right)_\rho d^3\mathbf{r} \quad . \quad (\text{B.11})$$

Eq. (3.24) follows at once.

APPENDIX C: STRUTINSKY-INTEGRAL THEOREM

To derive Eqns. (3.16) and (3.17) we begin by noting that the exact HF energy of any finite nuclear system (nucleus or WS cell) for Skyrme forces and a Slater treatment of the Coulomb exchange energy can be written in the local form

$$E_{HF} \equiv E_{HF}[\rho, \tau, \mathbf{J}] = \int \mathcal{E} \{ \rho(\mathbf{r}), \nabla \rho(\mathbf{r}), \tau(\mathbf{r}), \mathbf{J}(\mathbf{r}) \} d^3\mathbf{r} \quad , \quad (\text{C.1})$$

where in terms of the exact HF s.p. functions $\phi_i^{HF}(\mathbf{r})$ (not to be confused with the eigenfunctions $\phi_i(\mathbf{r})$ of Eq. (3.18)) we have

$$\rho(\mathbf{r}) = \sum_i n_i |\phi_i^{HF}(\mathbf{r})|^2 \quad , \quad (\text{C.2a})$$

$$\tau(\mathbf{r}) = \sum_i n_i |\nabla \phi_i^{HF}(\mathbf{r})|^2 \quad (\text{C.2b})$$

and

$$\mathbf{J}(\mathbf{r}) = -i \sum_i n_i \phi_i^{HF*}(\mathbf{r}) \nabla \times \boldsymbol{\sigma} \phi_i^{HF}(\mathbf{r}) \quad ; \quad (\text{C.2c})$$

for simplicity we do not distinguish here between the two charge states. For the exact HF quantities $\rho(\mathbf{r}), \tau(\mathbf{r})$ and $\mathbf{J}(\mathbf{r})$ let us now write

$$\rho = \tilde{\rho} + \delta\rho \quad , \quad (\text{C.3a})$$

$$\tau = \tilde{\tau} + \delta\tau \quad (\text{C.3b})$$

and

$$\mathbf{J} = \tilde{\mathbf{J}} + \delta\mathbf{J} \quad , \quad (\text{C.3c})$$

where $\tilde{\rho}, \tilde{\tau}$ and $\tilde{\mathbf{J}}$ represent the smooth quantities emerging from the (T)ETF calculation. Then to first order in $\delta\rho, \delta\tau$ and $\delta\mathbf{J}$ we have

$$\begin{aligned} E_{HF} = & \int \mathcal{E} \left\{ \tilde{\rho}(\mathbf{r}), \nabla \tilde{\rho}(\mathbf{r}), \dots, \tilde{\tau}(\mathbf{r}), \tilde{\mathbf{J}}(\mathbf{r}) \right\} d^3\mathbf{r} \\ & + \int \left\{ \left(\frac{\delta \mathcal{E}}{\delta \rho} \right)_{\tilde{\rho}, \tilde{\tau}, \tilde{\mathbf{J}}} \delta\rho + \left(\frac{\delta \mathcal{E}}{\delta \tau} \right)_{\tilde{\rho}, \tilde{\tau}, \tilde{\mathbf{J}}} \delta\tau + \left(\frac{\delta \mathcal{E}}{\delta \mathbf{J}} \right)_{\tilde{\rho}, \tilde{\tau}, \tilde{\mathbf{J}}} \cdot \delta\mathbf{J} \right\} d^3\mathbf{r} \quad , \end{aligned} \quad (\text{C.4})$$

where for the functional derivatives appearing here we have

$$\left(\frac{\delta\mathcal{E}}{\delta\rho}\right)_{\tilde{\rho},\tilde{\tau},\tilde{\mathbf{J}}} = \tilde{U}(\mathbf{r}) \quad , \quad (\text{C.5a})$$

$$\left(\frac{\delta\mathcal{E}}{\delta\tau}\right)_{\tilde{\rho},\tilde{\tau},\tilde{\mathbf{J}}} = \frac{\hbar^2}{2\widetilde{M^*}(\mathbf{r})} \quad (\text{C.5b})$$

and

$$\left(\frac{\delta\mathcal{E}}{\delta\mathbf{J}}\right)_{\tilde{\rho},\tilde{\tau},\tilde{\mathbf{J}}} = \tilde{\mathbf{W}}(\mathbf{r}) \quad , \quad (\text{C.5c})$$

in which $\tilde{U}, \hbar^2/(2\widetilde{M^*})$ and $\tilde{\mathbf{W}}$ are the smoothed ETF fields appearing in Eq. (3.18). Thus Eq. (C.4) becomes

$$E_{HF} = E_{ETF} + \int \left\{ \tilde{U}(\mathbf{r})\delta\rho + \frac{\hbar^2}{2\widetilde{M^*}(\mathbf{r})}\delta\tau + \tilde{\mathbf{W}}(\mathbf{r}) \cdot \delta\mathbf{J} \right\} d^3\mathbf{r} \quad . \quad (\text{C.6})$$

Comparing with Eq. (3.16), we see that we now have to identify the integral in this last equation with the shell correction E_{sc} of Eq. (3.17).

We next replace the exact HF s.p. functions $\phi_i^{HF}(\mathbf{r})$ in Eqns. (C.2a), (C.2b) and (C.2c) by the eigensolutions $\phi_i(\mathbf{r})$ to Eq. (3.18), and define thereby the quantities ρ', τ' and \mathbf{J}' , respectively; these quantities will certainly be fluctuating. We can then write

$$\delta\rho = (\rho' - \tilde{\rho}) + (\rho - \rho') \quad , \quad (\text{C.7})$$

and likewise for $\delta\tau$ and $\delta\mathbf{J}$. We recall now that $\tilde{\rho}$ is the initial approximation (ETF) to the exact HF density ρ , while ρ' represents our attempt to improve on this approximation. Thus the first term on the right-hand side of Eq. (C.7) can be regarded as the first-order estimate of the correction to $\tilde{\rho}$, while the second term represents the residual error. Accepting, then, that our method is essentially one of first-order perturbation theory, we simply drop the second term of Eq. (C.7). Treating $\delta\tau$ and $\delta\mathbf{J}$ in the same way, Eq. (C.6) reduces to

$$E_{HF} = E_{ETF} + \int \left\{ \tilde{U}(\mathbf{r})(\rho' - \tilde{\rho}) + \frac{\hbar^2}{2\widetilde{M^*}(\mathbf{r})}(\tau' - \tilde{\tau}) + \tilde{\mathbf{W}}(\mathbf{r}) \cdot (\mathbf{J}' - \tilde{\mathbf{J}}) \right\} d^3\mathbf{r} \quad . \quad (\text{C.8})$$

But it follows from Eq. (3.18) that

$$\int \left\{ \tilde{U}(\mathbf{r})\rho' + \frac{\hbar^2}{2\widetilde{M^*}(\mathbf{r})}\tau' + \tilde{\mathbf{W}}(\mathbf{r}) \cdot \mathbf{J}' \right\} d^3\mathbf{r} = \sum_i n_i \tilde{\epsilon}_i \quad . \quad (\text{C.9})$$

Then Eq. (C.8) reduces to

$$E_{HF} = E_{ETF} + \sum_i n_i \tilde{\epsilon}_i - \int \left\{ \tilde{U}(\mathbf{r}) \tilde{\rho} + \frac{\hbar^2}{2\tilde{M}^*(\mathbf{r})} \tilde{\tau} + \tilde{\mathbf{W}}(\mathbf{r}) \cdot \tilde{\mathbf{J}} \right\} d^3\mathbf{r} \quad . \quad (\text{C.10})$$

This completes the proof that to first order the shell correction is given by Eq. (3.17).

APPENDIX D: STRONG-DEGENERACY LIMIT OF THE TETF EXPANSION FOR ENTROPY

In the limit of low temperature and high density the TETF expansion of the entropy density σ_q is as follows. For the Thomas-Fermi approximation we have

$$\sigma_q^{(TF)} = \pi^2 \frac{M_q}{\hbar^2} \frac{1}{(3\pi^2 \rho_q)^{2/3}} \frac{\rho_q}{f_q} T + O(T^3) \quad . \quad (\text{D.1a})$$

The first-order correction in \hbar^2 to this is

$$\begin{aligned} \sigma_q^{(2)} = & -\frac{\pi^2}{27} \frac{M_q}{\hbar^2} \frac{1}{(3\pi^2 \rho_q)^{4/3}} \frac{1}{f_q} \left\{ \frac{(\nabla \rho_q)^2}{\rho_q} + \frac{9}{4} \rho_q \left(\frac{\nabla f_q}{f_q} \right)^2 + \frac{3}{f_q} \nabla \rho_q \cdot \nabla f_q \right\} T \\ & + O(T^3) \quad , \end{aligned} \quad (\text{D.1b})$$

while the second-order correction in \hbar^2 is

$$\sigma_q^{(4)} = -\frac{\pi^2}{1620} \frac{M_q}{\hbar^2} \frac{1}{(3\pi^2 \rho_q)^2} \left(17G_1^q - \frac{413}{12} G_2^q + \frac{47}{3} G_3^q \right) T + O(T^3) \quad . \quad (\text{D.1c})$$

In these equations we have defined $f_q = M_q/M_q^*$, while the G_i^q are defined in Eqns. (A.3a), (A.3b) and (A.3c).

-
- [1] M. Onsi, H. Przysiezniak and J. M. Pearson, Phys. Rev. C **55**, 3139 (1997).
 - [2] J. M. Lattimer, F. Mackie, D. G. Ravenhall and D. N. Schramm, Ap. J. **213**, 225 (1977).
 - [3] B. Meyer, Ap. J. **343**, 254 (1989).
 - [4] C. Freiburghaus, S. Rosswog and F.-K. Thielemann, Ap. J. **525**, L121 (1999).
 - [5] S. Goriely, P. Demetriou, H.-Th. Janka, J. M. Pearson and M. Samyn, Nucl. Phys. **A758**, 587c (2005).
 - [6] M. Arnould, S. Goriely and K. Takahashi, Phys. Reports **450**, 97 (2007).
 - [7] M. Ruffert and H.-Th. Janka, Astron. Astrophys. **380**, 544 (2001).

- [8] F. J. Dyson, *Nature* **223**, 486 (1969).
- [9] A. K. Harding and D. Lai, *Rep. Prog. Phys.* **69**, 2631 (2006).
- [10] P. Jaikumar, B. S. Meyer, K. Otsuki and R. Ouyed, *Astron. Astrophys.* **471**, 227 (2007).
- [11] K. Sumiyoshi, S. Yamada, H. Suzuki and W. Hillebrandt, *Astron. Astrophys.* **334**, 159 (1998).
- [12] C. J. Pethick and D. G. Ravenhall, *Ann. Rev. Nucl. Part. Sci.* **45**, 429 (1995).
- [13] F. Douchin and P. Haensel, *Phys. Lett. B* **485**, 107 (2000).
- [14] T. Maruyama, T. Tatsumi, D. N. Voskresensky, T. Tanigawa and S. Chiba, *Phys. Rev. C* **72**, 015802 (2005).
- [15] S. B. Rüster, M. Hempel and J. Schaffner-Bielich, *Phys. Rev. C* **73**, 035804 (2006).
- [16] P. Möller, J. R. Nix, W. D. Myers and W. J. Swiatecki, *At. Data Nucl. Data Tables* **59**, 185 (1995).
- [17] S. Goriely, M. Samyn and J. M. Pearson, *Phys. Rev. C* **75**, 064312 (2007).
- [18] D. Lunney, J. M. Pearson and C. Thibault, *Rev. Mod. Phys.* **75**, 1021 (2003).
- [19] J. M. Pearson and S. Goriely, *Nucl. Phys.* **A777**, 623 (2006).
- [20] G. Baym, C. Pethick and P. Sutherland, *Ap. J.* **170**, 299 (1971).
- [21] R. C. Tolman, *Phys. Rev.* **55**, 364 (1939).
- [22] J. R. Oppenheimer and G. M. Volkoff, *Phys. Rev.* **55**, 374 (1939).
- [23] J. M. Lattimer and F. D. Swesty, *Nucl. Phys.* **A535**, 331 (1991).
- [24] W. D. Myers and W. J. Swiatecki, *Nucl. Phys.* **81**, 1 (1966).
- [25] P. Bonche and D. Vautherin, *Nucl. Phys.* **A372**, 496 (1981).
- [26] J. W. Negele and D. Vautherin, *Nucl. Phys.* **A207**, 298 (1973).
- [27] A. Bulgac and P. Magierski, *Nucl. Phys.* **A683**, 695 (2001).
- [28] P. Magierski and P.-H. Heenen, *Phys. Rev. C* **65**, 045804 (2002).
- [29] P. Magierski, A. Bulgac and P.-H. Heenen, *Nucl. Phys.* **A719**, 217c (2003).
- [30] N. Chamel, S. Naimi, E. Khan and J. Margueron, *Phys. Rev. C* **75**, 055806 (2007).
- [31] K. Oyamatsu and M. Yamada, *Nucl. Phys.* **A578**, 181 (1994).
- [32] N. Chamel, *Nucl. Phys.* **A773**, 263 (2006).
- [33] M. Baldo, E. E. Saperstein and S. V. Tolokonnikov, *Nucl. Phys.* **A775**, 235 (2006).
- [34] A. K. Dutta, J.-P. Arcoragi, J. M. Pearson, R. Behrman and F. Tondeur, *Nucl. Phys.* **A458**, 77 (1986).
- [35] F. Tondeur, A. K. Dutta, J. M. Pearson and R. Behrman, *Nucl. Phys.* **A470**, 93 (1987).

- [36] J. M. Pearson, Y. Aboussir, A. K. Dutta, R. C. Nayak, M. Farine and F. Tondeur, Nucl. Phys. **A528**, 1 (1991).
- [37] Y. Aboussir, J. M. Pearson, A. K. Dutta and F. Tondeur, Nucl. Phys. **A549**, 155 (1992).
- [38] Y. Aboussir, J. M. Pearson, A. K. Dutta and F. Tondeur, At. Data Nucl. Data Tables **61**, 127 (1995).
- [39] A. K. Dutta, M. Onsi and J. M. Pearson, Phys. Rev. C **69**, 052801(R) (2004).
- [40] L. G. Cao, U. Lombardo, C. W. Shen and Nguyen Van Giai, Phys. Rev. C **73**, 014313 (2006).
- [41] B. Friedman and V. R. Pandharipande, Nucl. Phys. **A361**, 502 (1981).
- [42] W. Kohn and L. J. Sham, Phys. Rev. **140**, A1133 (1966).
- [43] J. Bartel, M. Brack and M. Durand, Nucl. Phys. **A445**, 263 (1985).
- [44] M. Farine, J. M. Pearson and F. Tondeur, Nucl. Phys. **A696**, 396 (2001).
- [45] Y. H. Chu, B. K. Jennings and M. Brack, Phys. Lett. B **68**, 407 (1977).
- [46] E. Chabanat, P. Bonche, P. Haensel, J. Meyer and R. Schaeffer, Nucl. Phys. **A635**, 231 (1998).
- [47] F. Douchin and P. Haensel, Astron. Astrophys. **380**, 151 (2001).
- [48] W. H. Press, S. A. Teukolsky, W. T. Vetterling and B. P. Flannery, *Numerical Recipes in Fortran* (2nd. edition). Cambridge University Press (1992). pp. 644-9.
- [49] C. J. Adkins, *Equilibrium Thermodynamics* (3rd. edition). Cambridge University Press (1983). pp. 181-2.
- [50] A. Weiss, W. Hillebrandt, H.-C. Thomas and H. Ritter, *Cox and Giuli's Principles of Stellar Structure*, extended second edition. Cambridge Scientific Publishers (2004).
- [51] M. Bender, P.-H. Heenen and P.-G. Reinhard, Rev. Mod. Phys. **75**, 121 (2003).

TABLE I: Convergence of the TETF expansion at $\bar{\rho} = 0.06$ nucleons.fm $^{-3}$ for cell with $Z = 30$, $A = 1123$. Temperature T in MeV.

T	0.1	1.0	3.0
ϕ_n	0.1943E+02 -0.1027E-01 19.42 0.3566E-03	0.1934E+02 -0.9452E-02 19.33 0.2959E-03	0.1845E+02 -0.3529E-02 18.45 0.8834E-04
ϕ_p	0.1818 0.3598E-02 0.1877 0.2299E-02	0.1659E+00 0.5124E-02 0.1724 0.1404E-02	-0.2328E-01 0.2516E-02 -0.02054 0.2167E-03
s_n	0.1477E-01 -0.1387E-05 0.01477 -0.3124E-07	0.1476E+00 -0.1318E-04 0.1476 -0.2757E-06	0.4401E+00 -0.1879E-04 0.4401 -0.3389E-06
s_p	0.2110E-02 -0.1537E-02 -1.005E-03 -0.1578E-02	0.1695E-01 -0.2133E-02 0.01516 0.3437E-03	0.6378E-01 -0.4283E-03 0.06337 0.2441E-04
$s_p^{s.p.}$	0.0036233	0.01646	0.06446
$c_{v,n}$	0.1477E-01 -0.1388E-05 0.01477 -0.3125E-07	0.1473E+00 -0.1352E-04 0.1473 -0.2880E-06	0.4316E+00 -0.2503E-04 0.4316 -0.5186E-06
$c_{v,p}$	0.1895E-02 -0.9657E-03 0.0075 0.6571E-02	0.1372E-01 0.4703E-03 0.01379 -0.4022E-03	0.3366E-01 0.4400E-03 0.03410 -0.2655E-05

TABLE II: Convergence of the TETF expansion at $\bar{\rho} = 3 \times 10^{-4}$ nucleons.fm $^{-3}$ for cell with $Z = 40, A = 150$. Temperature T in MeV.

T	0.1	1.0	3.0
ϕ_n	0.1472E+02 -0.2021E+00 14.57 0.4855E-01	0.1164E+02 -0.1824E+00 11.52 0.5564E-01	-0.2114E+01 -0.5707E-01 -2.135 0.3647E-01
ϕ_p	0.4465E+01 -0.3411E-01 4.496 0.6509E-01	0.4699E+01 -0.3642E-01 4.727 0.6379E-01	0.6777E+00 -0.1831E-01 0.6960 0.3655E-01
s_n	0.2082E+00 -0.8479E-02 0.1936 -0.6098E-02	0.1026E+01 -0.2113E-01 1.006 0.1083E-02	0.2923E+01 -0.1382E-01 2.909 0.1035E-03
s_p	0.7193E-02 -0.1315E-01 0.01024 0.1620E-01	0.6150E-01 -0.2234E-01 0.0405 0.1303E-02	0.8998E+00 -0.1353E-01 0.8864 0.1074E-03
$s_p^{s.p.}$	0.1199E-03	0.06322	0.7088
$c_{v,n}$	0.1385E+00 -0.6991E-02 0.1410 0.9451E-02	0.3958E+00 -0.4233E-02 0.3905 -0.1176E-02	0.8998E+00 0.1726E-02 0.9015 -0.1625E-03
$c_{v,p}$	0.6965E-02 -0.4111E-02 -0.00867 -0.1152E-01	0.5660E-01 -0.2989E-02 0.05094 -0.2666E-02	0.2593E+00 0.2649E-02 0.2619 -0.3149E-04

TABLE III: TETFSI results for number of protons Z and total number of nucleons A in WS cell for nuclear and beta equilibrium at $T = 0$ as a function of $\bar{\rho}$ for force BSK14. TETF results in parentheses. Last two columns show TETFSI values of pressure P and $\left(\frac{\partial P}{\partial T}\right)_{\bar{\rho}}$

$\bar{\rho}$ (fm ⁻³)	Z	A	P (MeV.fm ⁻³)	$\left(\frac{\partial P}{\partial T}\right)_{\bar{\rho}}$ (fm ⁻³)
0.0003	50 (38)	200 (146)	0.000940	0
0.001	50 (39)	460 (385)	0.00179	0
0.005	50 (39)	1140 (831)	0.00813	0
0.01	40 (38)	1215 (1115)	0.0185	0
0.02	40 (35)	1485 (1302)	0.0448	0
0.03	40 (33)	1590 (1303)	0.0784	0
0.04	40 (31)	1610 (1261)	0.121	0
0.05	20 (30)	800 (1171)	0.175	0
0.06	20 (29)	780(1105)	0.243	0

TABLE IV: As for Table III but with $T = 0.1$ MeV.

$\bar{\rho}$ (fm ⁻³)	Z	A	P (MeV.fm ⁻³)	$\left(\frac{\partial P}{\partial T}\right)_{\bar{\rho}}$ (fm ⁻³)
0.0003	50 (38)	200 (147)	0.000946	0.0000423
0.001	50 (39)	460 (341)	0.00179	0.000140
0.005	50 (38)	1130 (842)	0.00816	0.000270
0.01	40 (38)	1210 (1107)	0.0185	0.000346
0.02	40 (35)	1480 (1294)	0.0448	0.000444
0.03	40 (33)	1595 (1303)	0.0784	0.000511
0.04	40 (31)	1610 (1242)	0.121	0.000568
0.05	20 (30)	800 (1190)	0.175	0.000617
0.06	20 (29)	765 (1116)	0.243	0.000662

TABLE V: As for Table III but with $T = 1.0$ MeV.

$\bar{\rho}$ (fm ⁻³)	Z	A	P (MeV.fm ⁻³)	$\left(\frac{\partial P}{\partial T}\right)_{\bar{\rho}}$ (fm ⁻³)
0.0003	46 (37)	310 (234)	0.000633	0.000182
0.001	46 (38)	520 (450)	0.00192	0.000631
0.005	44 (39)	1020 (858)	0.00936	0.00233
0.01	42 (37)	1280 (1120)	0.0202	0.00329
0.02	40 (36)	1480 (1307)	0.04701	0.00434
0.03	38 (33)	1505 (1301)	0.0810	0.00502
0.04	36 (31)	1450 (1232)	0.124	0.00553
0.05	34 (30)	1340 (1165)	0.179	0.00568
0.06	26 (29)	985 (1082)	0.246	0.00445

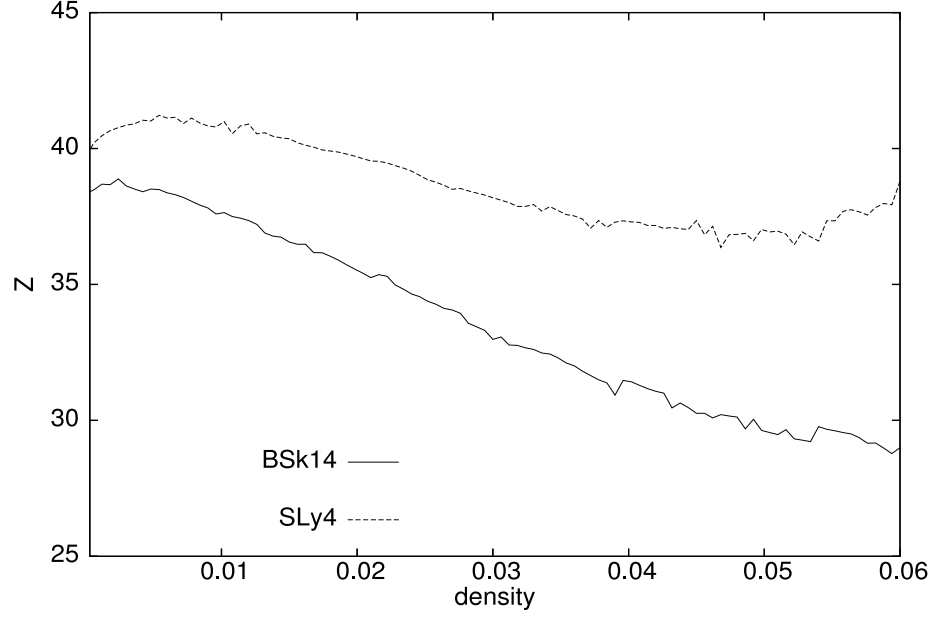


FIG. 1: Number of protons Z in WS cell given by ETF method for nuclear and beta equilibrium at $T = 0$ as a function of density (fm^{-3}) for forces BSk14 and SLy4.

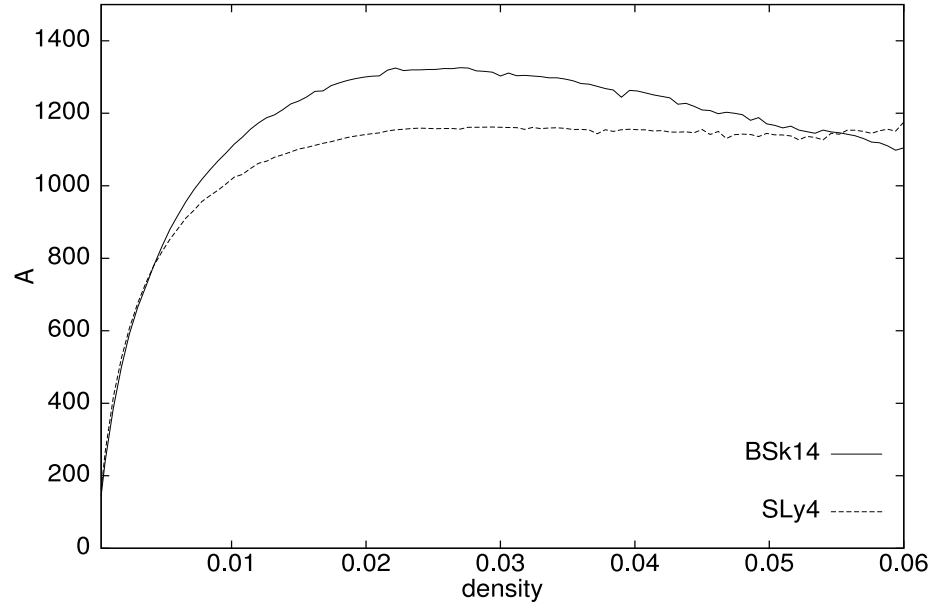


FIG. 2: Total number of nucleons $A = Z + N$ in WS cell given by ETF method for nuclear and beta equilibrium at $T = 0$ as a function of density (fm^{-3}) for forces BSk14 and SLy4.

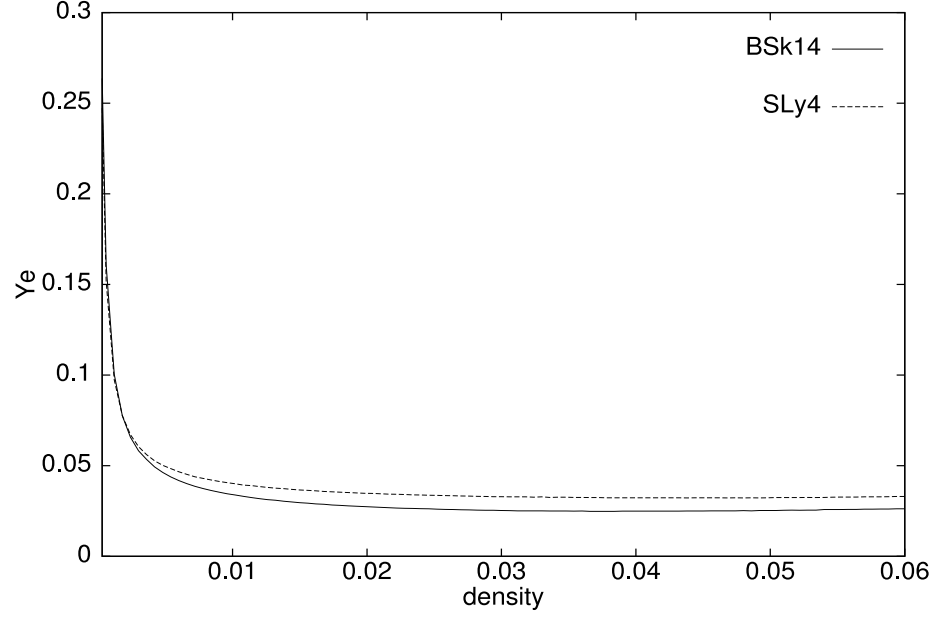


FIG. 3: Fraction $Y_e = Z/A$ of nucleons that are protons given by ETF method for nuclear and beta equilibrium at $T = 0$ as a function of density (fm^{-3}) for forces BSk14 and SLy4.

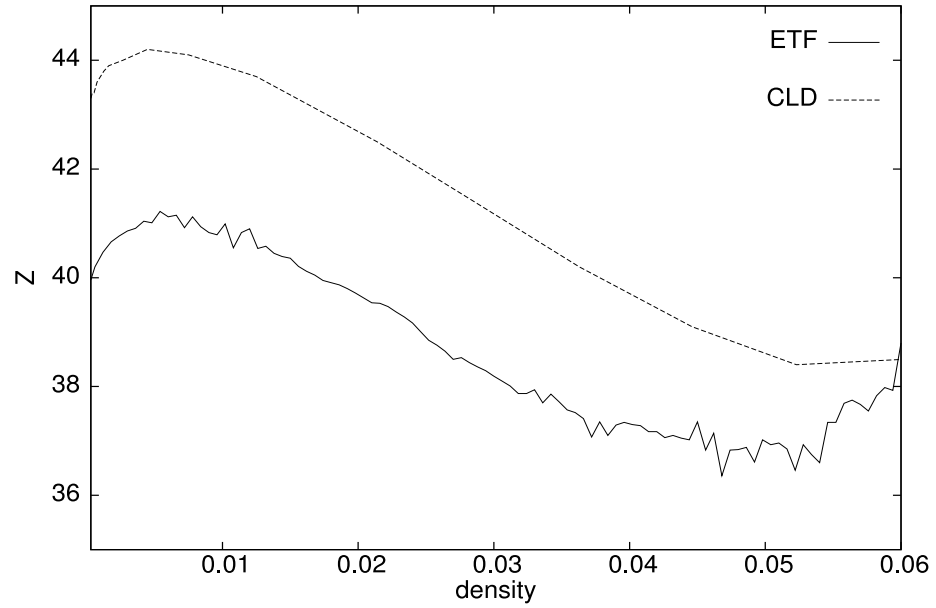


FIG. 4: Comparison of ETF and CLD (compressible liquid drop) calculations of equilibrium value of Z at $T = 0$ as a function of density (fm^{-3}) with SLy4 force.

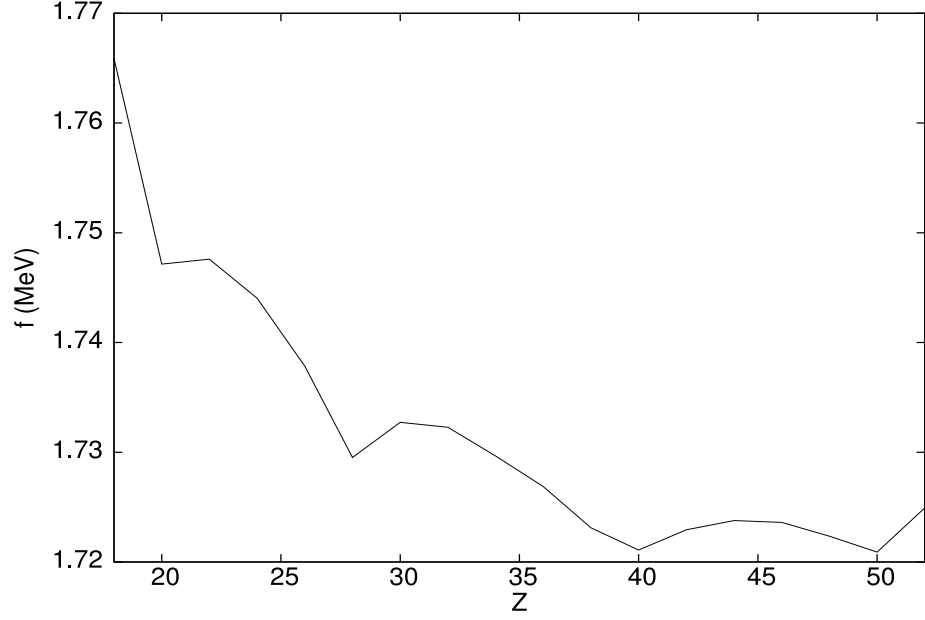


FIG. 5: Variation of f_{TETFSI} with Z (always for optimal value of A) at $\bar{\rho} = 0.005 \text{ fm}^{-3}$ and $T = 0.1 \text{ MeV}$.

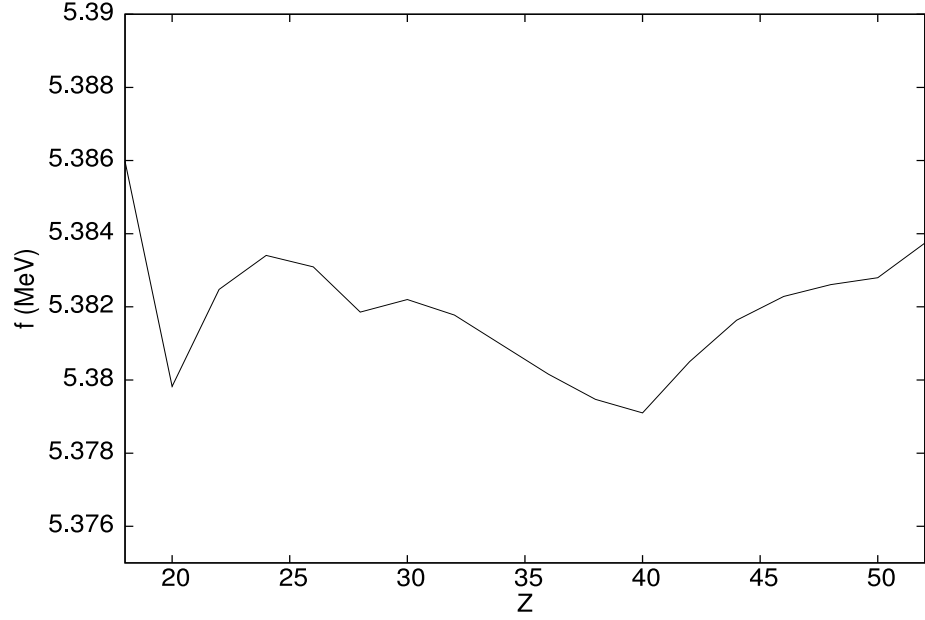


FIG. 6: Variation of f_{TETFSI} with Z (always for optimal value of A) at $\bar{\rho} = 0.04 \text{ fm}^{-3}$. and $T = 0.1 \text{ MeV}$.